© 2019. Published by The Company of Biologists Ltd | Journal of Experimental Biology (2019) 222, jeb191544. doi:10.1242/jeb.191544

RESEARCH ARTICLE

Encoding phase spectrum for evaluating 'electric qualia'

Angel Ariel Caputi* and Pedro Aníbal Aguilera

ABSTRACT

The most broadly expressed and studied aspect of sensory transduction is receptor tuning to the power spectral density of the incoming signals. Temporal cues expressed in the phase spectrum are relevant in African and American pulse-emitting electric fish showing electroreceptors sensing the signals carried by the self- and conspecific-generated electric organ discharges. This article concerns the role of electroreceptor phase sensitivity in American pulse Gymnotiformes. These fish show electroreceptors sharply tuned to narrow frequency bands. This led to the common thought that most electrosensory information is contained in the amplitude spectra of the signals. However, behavioral and modeling studies suggest that in their pulses, Gymnotiformes electroreceptors also encode cues embodied in the phase spectrum of natural stimuli. Here, we show that the two main types of tuberous primary afferents of *Gymnotus omarorum* differentially respond to cues embodied in the amplitude and phase spectra of self-generated electrosensory signals. One afferent type, pulse markers, is mainly driven by the amplitude spectrum, while the other, burst coders, is predominantly sensitive to the phase spectrum. This dual encoding strategy allows the fish to create a sensory manifold where patterns of 'electric color' generated by object impedance and other potential sources of 'colored' images (such as large nearby objects and other electric fish) can be represented.

KEY WORDS: Electric image, Electroreceptors, Latency code, Burst code, Electric color

INTRODUCTION

Sensory signals can be defined as modulations of energy carriers sensed by mosaics of receptors specifically tuned to a type of energy (Müller, 1837). Receptor sensitivity to stimulus frequency is usually not uniform and often different receptor types sense different aspects of the stimuli (Wald, 1964; Hudspeth, 1989). While the energy pattern that directly drives sensory receptors is referred to as the 'proximal stimulus', the actual or apparent source of such energy patterns is called the 'distal stimulus' (Palmer, 1999). Distal stimulus location and spatial qualities (i.e. size, shape and orientation) are usually carried by the proximal stimulus pattern over the sensory mosaic, whereas qualitative aspects such as color or texture are often related to the responsiveness of different receptor types to the proximal stimulus. While the most studied aspect of qualitative encoding of the stimulus is the response of receptor types to the power spectral density, less attention has been paid to the effects of the phase spectrum. The two main groups of pulse-emitting weakly electric teleosts (Mormyridea from Africa and Gymnotiformes from America) are a good model to study this last issue. The ability to sense the entire time course of allo- and self-generated transcutaneous electrical fields including the amplitude and phase spectra was behaviorally shown in pulse Gymnotiformes (Heiligenberg and Altes, 1978) and pulse Mormyriformes (Hopkins and Baas, 1981).

Cues embodied in the changes of the phase spectra of the species-specific allo- and self-generated electric fields are relevant in pulse-emitting Mormyriformes for species and sex identification (Hopkins and Baas, 1981; Hopkins, 1986) and also to discriminate object impedance (von der Emde, f1990; von der Emde and Bleckmann, 1992; Gottwald et al., 2018). These teleosts possess an electrosensory path to sense the discharge of other fish (Bell and Grant, 1989). This path originates in the so-called knollenorgan receptors, which are mainly sensitive to the phase spectrum of the conspecific electric organ discharge (EOD) (Hopkins and Bass, 1981; Hopkins, 1986). There is another path originating in complex 'mormyromast receptors' innervated by two different types of fibers (Bell, 1990a, b) that show 'wide band' responsiveness to the amplitude spectrum (Bennett, 1967; Bell, 1990a, b). While one type of mormyromast-innervating fibers is only sensitive to stimulus strength, the other also responds to phase spectrum (von der Emde and Bleckmann, 1992). This dual (strength and phase) encoding has been related to impedance discrimination (von der Emde, 1990; von der Emde and Ronacher, 1994). Although two parameters are not enough to determine the impedance of an object, it has been shown that one can define families of impedance values that, independently of their position, modify reafferent signals in such a way that phase and strength are related by a linear function, defining an electric qualia likened to 'electric color' (Budelli and Caputi, 2000). Recent experimental evidence supports this hypothesis (Gottwald et al., 2018).

In contrast, pulse-emitting Gymnotiformes discharge brief waveforms consisting of a traveling wave along the body (Gymnotidae: Bennett and Grundfest, 1959; Caputi, 1999, Assad et al., 1999; Rodríguez-Cattáneo et al., 2008, 2013; Castelló et al., 2009; Rhamphychtidae: Caputi et al., 1994, Hypoppomidae: Caputi et al., 1998; Stoddard et al., 1999; Waddell et al., 2016). As the near field in the fish neighborhood shows site- and time-dependent amplitude and orientation, any object (either purely resistive or having complex impedance) introduces changes in the strength and time course (i.e. amplitude and phase spectrum) of transcutaneous currents (Pereira and Caputi, 2010). These changes in the local stimulus waveforms are encoded at the primary afferent level (Rodríguez-Cattáneo et al., 2017), allowing object (Aguilera and Caputi, 2003) and individual discrimination (McGregor and Westby, 1992). In fact, within the range 1–30 nF, capacitive objects alter the time course of the local transcutaneous currents, provoking a shift in the amplitude spectra [$H(\omega)$] to a higher frequency range and also a lag of the lower frequency components of the phase spectra [$\theta(\omega)$; Aguilera and Caputi, 2003; Rodríguez-Cattáneo et al., 2017). These changes in the local stimulus cause a strong reduction of the latency

Departamento de Neurociencias Integrativas y Computacionales, Instituto de Investigaciones Biológicas Clemente Estable, CP 11600, Montevideo, Uruguay.

*Author for correspondence (acaputi@iibce.edu.uy)

A.A.C., 0000-0002-7238-0538; P.A.A., 0000-0002-6610-4895

Received 30 August 2018; Accepted 14 January 2019

Journal of Experimental Biology (2019) 222, jeb191544. doi:10.1242/jeb.191544

List of symbols and abbreviations

BC	burst coder
EOD	electric organ discharge
FFT	fast Fourier transform
$H_C(\omega)$	capacitive amplitude spectrum
$H_C\theta_0(t)$	waveform with capacitive amplitude and zero-phase spectra
$H_C\theta_C(t)$	natural waveform in the presence of a capacitive object
$H_C\theta_R(t)$	transposed waveform with capacitive amplitude and resistive phase spectra
$H_R(\omega)$	resistive amplitude spectrum
$H_R\theta_0(t)$	waveform with resistive amplitude and zero-phase spectra
$H_R\theta_C(t)$	transposed waveform with resistive amplitude and capacitive phase spectra
$H_R\theta_R(t)$	natural waveform in the presence of a resistive object
iFFT	inverse fast Fourier transform
P_{HB}	significance level after Holm–Bonferroni's correction for multiple comparisons
PM	pulse marker
rms	root mean squared
ROC	receiver operating characteristic
$\theta_0(\omega)$	zero-phase spectrum
$\theta_C(\omega)$	capacitive phase spectrum
$\theta_R(\omega)$	resistive phase spectrum

and inter-spike interval as well as an increase in the number of spikes of the responses of one type of primary electroreceptor afferent (Rodríguez-Cattáneo et al., 2017). In addition, changes in the relative orientation of another electric fish cause changes in the received transcutaneous stimulus waveform, in particular when the two animals are close to each other (Aguilera et al., 2001). Behavioral evidence indicates that *Gymnotus omarorum* are able to discriminate between objects of different impedance (Aguilera and Caputi, 2003) and between members of the same genus showing a difference in head to tail waveform (McGregor and Westby, 1992).

Pulse Gymnotiformes show two main types of primary electrosensory afferents, pulse markers (PMs) and burst coders (BCs) (Szabó and Fessard, 1974; Zakon, 1986; Kawasaki, 2005). Each electroreceptor organ is innervated by a single fiber (Szabó and Fessard, 1974; Zakon, 1986; Kawasaki, 2005; Echagüe and Trujillo-Cenóz, 1981; Caputi et al., 2002), the response of which (as in wave fish; Scheich et al., 1973; Hopkins, 1976) is sharply tuned to a narrow frequency band falling within the range of the power spectral density of the species-specific EOD (Bastian, 1976; 1977; Watson and Bastian, 1979; McKibben et al., 1993; Yager and Hopkins, 1993; Zakon, 1986; Kawasaki, 2005). Although it is usually accepted that most electrosensory information driving the above-mentioned behaviors is contained in the amplitude spectra of the proximal electrosensory stimuli, behavioral (Heiligenberg and Altes, 1978), physiological (Bennett, 1967; Hopkins and Westby, 1986; McKibben et al., 1993) and modeling (Bennett, 1967) studies suggest that in pulse Gymnotiformes, electroreceptors may also encode cues embodied in the time course of self- and allo-generated stimuli. A more recent model (Cilleruelo and Caputi, 2012) suggests that BC subpopulations previously described (Bastian, 1976, 1977; Watson and Bastian, 1979; Yager and Hopkins, 1993; McKibben et al., 1993) might represent examples from a continuum of receptors of different size (Viancour, 1979) and that at least a subpopulation would be able to respond differently to signals having the same power spectral density but different phase spectrum.

Here, we investigated amplitude and phase encoding by testing: (i) whether changes in time course without changes in the power spectral density are sensed by PM and BC primary afferents and (ii) the difference in sensitivity of PMs and BCs to the $H(\omega)$ and $\theta(\omega)$ spectra of the self-generated stimuli. We show that the two types of tuberous primary afferents of the pulse-emitting fish *G. omarorum* respond differently to amplitude and phase cues as well as to the total energy of the signal. PMs are mainly driven by the amplitude spectrum while BCs are predominantly sensitive to the phase spectrum.

MATERIALS AND METHODS

Experiments were performed in three adult *Gymnotus omarorum* length: 15, 19 and 21 cm, unidentified sex; species described by Richer-de-Forges et al., 2009; genotyped by Eastman et al., 2018; and held by Jason Gallant at http://efishgenomics.integrativebiology.msu.edu/). Fish were gathered during the 2017–2018 summer season in Laguna del Cisne, Departamento de Maldonado, República Oriental del Uruguay, coordinates 34.848846 S, 55.117762 W. Individuals were individually maintained in separate aquaria and fed with insect larvae. Conductivity was kept at 100 µS cm^{-1}. Temperature was controlled between 19 and 23°C during captivity. All surgical maneuvers were performed in anesthetized fish not responding to noxious stimuli or in 'brain dead' fish after decerebration (protocol 001/003/2011 of the animal care committee of the Instituto de Investigaciones Biológicas Clemente Estable).

Surgery

Prior to the surgery, specimens were immersed in cold water and small pieces of ice were successively added to reduce the water temperature until the fish stopped its EOD, lost its balance and was not responsive to pinpricking. At this point, the fish was placed into a cellulose sponge holder, and a small drop of lidocaine gel was applied to the scalp before surgery. After removing the scalp, another drop of lidocaine gel was applied on the exposed bone and two lateral holes were drilled on the skull projection of the telencephalon. Decerebration was carried out by completely removing the telencephalon through the left hole using a vacuum probe (Rodríguez-Cattáneo et al., 2017). The recording tank (40×60 cm) in which decerebration was rapidly completed was filled to a depth of 5 cm with cold water (10°C, 100 µS cm^{-1}). The skulls of decerebrate animals were firmly attached to a plastic holder with a nichrome wire passing through both skull holes. The wires and holder were embedded with a mix of dental cement and cyanoacrylate to make a strong bond with the skull. The body was maintained aligned to the center of the tank by passing a silk thread through the dorsal body mass along the longitudinal axis of the fish. At the posterior limit of the skull, the muscles were separated to expose the first and second vertebrae. At this level, the spinal cord was sectioned through a laminectomy and the wound was closed with stitches and cyanoacrylate. Experiments were carried out at about 23°C.

Experimental design and hypotheses

The following hypotheses for explaining the ability of electroreceptors to respond with shorter latencies and stronger bursts to changes in stimulus waveform without a change in strength were put forward previously (Rodríguez-Cattáneo et al., 2017). Electroreceptors respond differentially to: (i) the amplitude spectrum of the local EODs stimulating receptors facing either resistive or capacitive objects [referred to as $H_R(\omega)$ and $H_C(\omega)$, respectively]; (ii) the phase spectrum of the same signals [referred to as $\theta_R(\omega)$ and $\theta_C(\omega)$, respectively]; or (iii) both spectra.

Power spectral densities of natural capacitive and resistive stimuli largely overlap (Aguilera and Caputi, 2003; Rodríguez-Cattáneo et al., 2013) but their phase spectra are different. The effect of these

Journal of Experimental Biology (2019) 222, jeb191544. doi:10.1242/jeb.191544

natural signals was contrasted with those of signals that for each amplitude spectrum had either the same but transposed phase spectrum or a flat zero-phase spectrum. Capacitive phase-resistive amplitude and resistive phase-capacitive amplitude will be in general referred to as transposed stimuli. To evaluate the effect of amplitude spectra alone, we recorded the responses to zero-phase stimuli in which the phase of all frequency components was the same. To evaluate the presence of an effect of the phase spectra, we compared responses obtained with natural, zero-phase and transposed stimuli (i.e. exchanging phase spectra while maintaining amplitude spectra).

Stimulus battery

To construct the appropriate waveforms (illustrated in Figs 1A and 3A, insets) for testing the above-posed hypotheses, two 'natural' self-generated fields having the same equal total energy [i.e. root mean squared (rms) value] were recorded in the presence of a resistor [10 kΩ, $H_R\theta_R(t)$] and a capacitor [10 nF, $H_C\theta_C(t)$] (data obtained from Rodríguez-Cattáneo et al., 2017). The fast Fourier transforms (FFTs) of natural waveforms were calculated, the amplitude and phase components were modified as defined below, and finally the stimuli were calculated as follows, using the inverse fast Fourier transform (iFFT) (where j is the imaginary unit in the field of complex numbers):

Natural resistive signals: $H_R(\omega) \times e^{j\theta_R(\omega)} = \mathrm{FFT}(H_R\theta_R(t))$

Natural capacitive signals: $H_C(\omega) \times e^{j\theta_C(\omega)} = \mathrm{FFT}(H_C\theta_C(t))$

Zero-phase, resistive amplitude: $H_R\theta_0(t) = \mathrm{iFFT}(H_R(\omega))$

Zero-phase, capacitive amplitude: $H_C\theta_0(t) = \mathrm{iFFT}(H_C(\omega))$

Capacitive phase, resistive amplitude: $H_R\theta_C(t) = H_R(\omega) \times e^{j\theta_C(\omega)}$

Resistive phase, capacitive amplitude: $H_C\theta_R(t) = H_C(\omega) \times e^{j\theta_R(\omega)}$.

Stimuli were applied between a bare tungsten wire inserted in the dorsal body muscles and a tungsten electrode in the water using a stimulus isolation unit (A-M Systems 2200, Sequim, WA, USA). The waveform was controlled by a computer program (Experimenter) through an analog to digital interface (Datawave, Colorado Springs, CO, USA). Amplitude was controlled by a rheostat that had its ends connected between the analog to digital output and the ground and its middle point connected to the stimulus isolation unit input. Responses to these stimuli were evaluated by playing blocks of either 250 or 1000 identical stimuli at 33 Hz for each waveform. All the stimulus waveforms used in the evaluation of a receptor had the same rms value.

Primary afferent recordings

'Michigan-type' electrodes (Neuro Nexus, Ann Arbor, MI, USA) with 16 on-beam recording spots were lowered through a craniotomy at the skull projection of the rostral region of the left electrosensory lobe where the afferent fibers enter the brain stem. Trains of action potentials in response to stimuli were recorded between the electrode recording spots and a reference in the cisterna magna connected to a multiplexed differential amplifier (A-M systems 3600), the output of which was digitized at a sampling frequency of 40 kHz using an analog to digital interface (Datawave) and processed with the aid of a sequence of commands (Experimenter, Datawave-associated software). Spike conditioning and selection were made off-line using a previously defined procedure (Pereira et al., 2014; Rodríguez-Cattáneo et al., 2017). To isolate a single afferent fiber, we first placed the stimulation electrode a couple of centimeters rostral to the most likely location and then moved the probe towards the skin, tracking the best response while reducing the stimulus intensity using the rheostat.

We identified PMs by checking that the response always consisted of a single spike of short latency (less than 3 ms) and

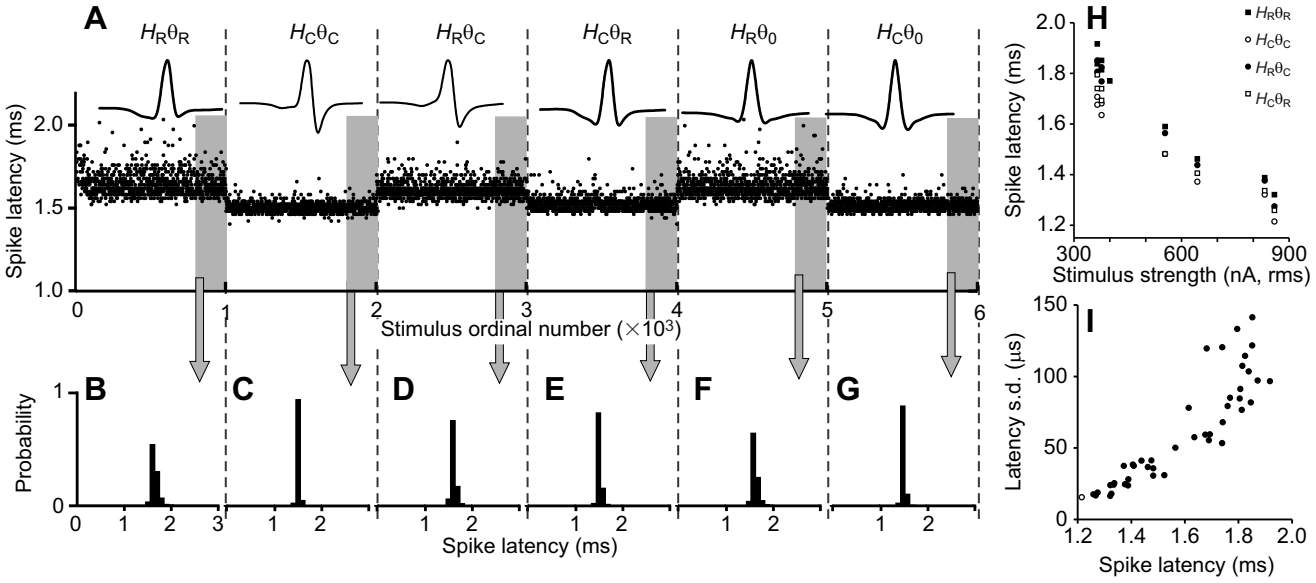

Fig. 1. Pulse marker (PM) responses. (A) Raster plot of a single PM receptor stimulated by successive trains of 1000 stimuli, the waveforms of which are represented in the insets. Dashed lines indicate the transition between trains. $H_R\theta_R$ and $H_C\theta_C$: natural stimuli in the presence of resistive or capacitive objects; $H_R\theta_C$ and $H_C\theta_R$: transposed stimuli in the presence of resistive or capacitive objects; $H_R\theta_0$ and $H_C\theta_0$: zero-phase stimuli in the presence of resistive or capacitive objects. (B–G) Post-stimulus histograms of the latencies (in this case, the last 250 stimuli were considered in each train; gray bands and arrows indicate correspondence). (H) Latency as a function of stimulus strength [root mean squared (rms) value]. Although every PM was only stimulated at a single amplitude, the curve shows a smooth hyperbolic shape. Note that open symbols are always below filled ones. (I) Latency variability as a function of latency (Spearmann correlation, ρ=0.9246).

Journal of Experimental Biology (2019) 222, jeb191544. doi:10.1242/jeb.191544

that a second spike did not fire when increasing the stimulus to an intensity equivalent to five times the threshold intensity (Rodríguez-Cattáneo et al., 2017). Stimulus intensity was kept constant for each receptor, varying from unit to unit, but always set below the saturation of spike latency. We identified BCs by the characteristic presence of a burst of spikes. The stimulus intensity was adjusted until the average number of spikes in response to a natural resistive stimulus was between 1 and 2.

Quantification and statistical analysis

Post-stimulus histograms were constructed for each unit. To minimize the spike firing adaptation effects, only the responses to the last stimuli for a given waveform were considered (the last 250 or 100 responses in the case of trains of 1000 or 250 stimuli, respectively, Figs 1A–G and 3A–G). The mean latency of the earliest spike (measured from the positive peak of the head to tail EOD to the main peak of the unit) was used to quantify the latency response of both afferent types. The rate (total number of spikes in the train over the number of stimuli) was also used to quantify the responses of BCs.

We used Friedman tests followed by exact tests to evaluate whether response parameters are systematically ordered according to stimulus type. This procedure eliminates the effects of stimulus strength and potential differences in threshold among different units belonging to different fish. Taking into account that either $H(\omega)$ or $\theta(\omega)$, or both, causes the stronger responses observed for natural capacitive stimuli (Rodríguez-Cattáneo et al., 2017), we used one-tail *post hoc* exact tests to compare (i) responses to stimuli sharing the same $H(\omega)$ and differentiated by their $\theta(\omega)$ and (ii) responses to stimuli sharing the same $\theta(\omega)$ and differentiated by their $H(\omega)$ (brackets in Figs 2, 4 and 5). To evaluate the relative weight of $H(\omega)$ and $\theta(\omega)$ on the responses, we pairwise compared the differences between the response parameters obtained with the stimuli having $H_C(\omega)$ and $H_R(\omega)$ for natural, zero-phase and transposed stimuli. Holm–Bonferroni's correction was systematically applied to avoid inflation of type I error; significance level after correction (referred to as P_{HB}) was 0.05 throughout. Finally, we constructed receiver operating characteristic (ROC) curves to evaluate, for each given response parameter, the ability of an external observer to discriminate between amplitude spectra (and between phase spectra) for a given receptor type. To test the consistency of these observations among recorded individual receptors, we performed Friedman tests followed by *post hoc* exact tests comparing the areas under the ROC curves obtained for each receptor and spike parameter.

RESULTS

We tested the hypothesis that the two afferent types encode the amplitude and phase spectra differently by recording unitary responses of primary afferents (7 PMs and 9 BCs in three decerebrated and spinalized fish) to trains of six synthesized waveforms equalized by their rms current intensity values played at a constant rate (33 Hz). Two of these waveforms reproduced 'natural' stimuli in the presence of resistive (10 kΩ) or capacitive (10 nF) objects (Aguilera and Caputi, 2003; Rodríguez-Cattáneo et al., 2017): $H_R\theta_R(t)$ and $H_C\theta_C(t)$, equivalent to $H_R(\omega)\times e^{j\theta_R(\omega)}$ and $H_C(\omega)\times e^{j\theta_C(\omega)}$ in the frequency domain, respectively. These signals were also used for constructing zero-phase [$H_R\theta_0(t)$ and $H_C\theta_0(t)$, defined as the inverse FFTs of $H_R(\omega)\times e^0$ and $H_C(\omega)\times e^0$] and transposed stimuli [$H_R\theta_C(t)$ and $H_C\theta_R(t)$, defined as the iFFTs of $H_R(\omega)\times e^{j\theta_C(\omega)}$ and $H_C(\omega)\times e^{j\theta_R(\omega)}$; see Materials and Methods].

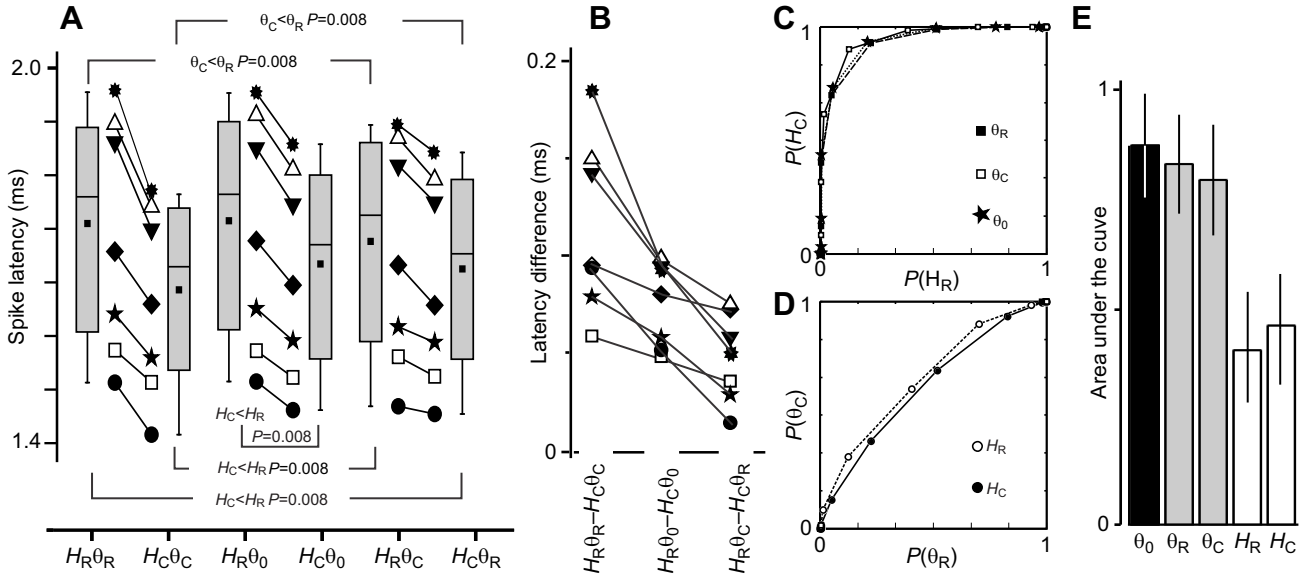

Fig. 2. PMs: population data. (A) Mean spike latency as a function of stimulus waveform (Friedman test, χ^2=34, d.f.=5, P=2.1×10^{-6}). *Post hoc* exact tests were performed to rule out the hypotheses: 'responses to stimuli having $\theta_R(\omega)$ have equal or smaller latency than those having $\theta_C(\omega)$' and 'responses to stimuli having $H_R(\omega)$ have equal or smaller latency than those having $H_C(\omega)$' (the five brackets indicate performed tests, P=0.0078, N=7). (B) Differences between mean spike latencies evoked by stimuli having $H_R(\omega)$ and $H_C(\omega)$ (Friedman test: χ^2=14, d.f.=2, P=9×10^{-4} followed by *post hoc* exact tests: P=0.0078, N=7, three tests; as indicated by the connecting lines in A). In A and B, symbols correspond to mean data for individually recorded units and the box and whisker plots are summaries. (C,D) Receiver operating characteristic (ROC) curves for the unit of Fig. 1. (C) Probability that the amplitude spectrum is $H_C(\omega)$ {$P[H_C(\omega)]$} as a function of the probability that it is $H_R(\omega)$ {$P[H_R(\omega)]$} when the spike has the same latency for stimuli with either $\theta_R(\omega)$ (black squares), $\theta_0(\omega)$ (stars) or $\theta_C(\omega)$ (white squares) phase spectra. (D) Probability that the phase spectrum is $\theta_C(\omega)$ {$P[\theta_C(\omega)]$} as a function of probability that it is $\theta_R(\omega)$ {$P[\theta_R(\omega)]$} when the spike has the same latency for stimuli with either $H_C(\omega)$ (black circles) or $H_R(\omega)$ (white circles) amplitude spectra. (E) Areas under the ROC curves for amplitude discrimination (gray and black bars) are significantly larger than those for phase discrimination (white bars, Friedman test: χ^2=21.8, d.f.=4, P=2×10^{-4}, followed by six *post hoc* exact tests: P=0.0078, N=7). Lines correspond to s.d. Numbers within the brackets in A are P-values before correction for multiple tests.

Journal of Experimental Biology (2019) 222, jeb191544. doi:10.1242/jeb.191544

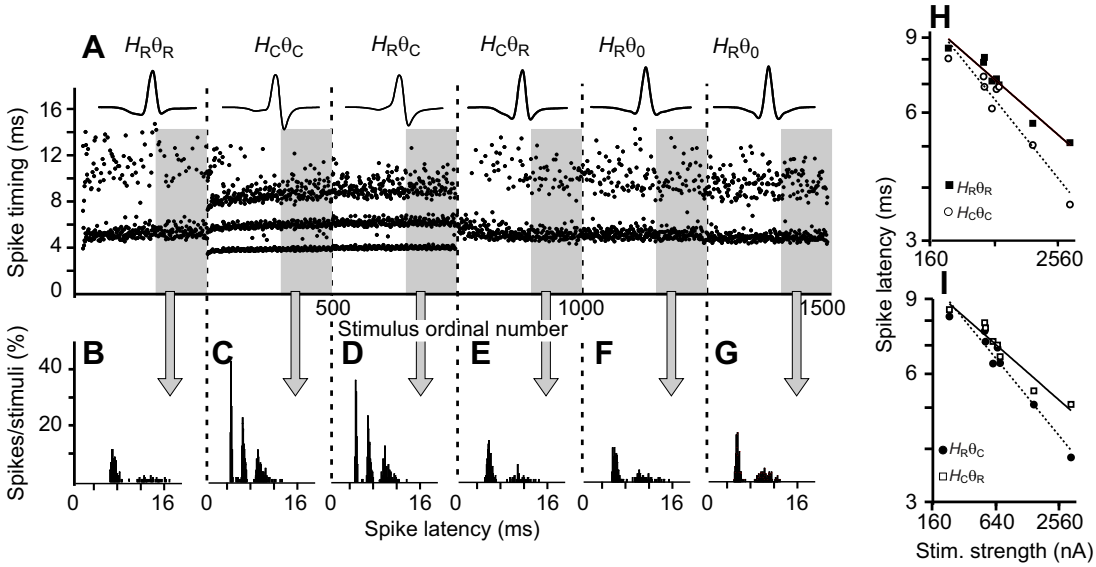

Fig. 3. Burst coder (BC) responses. (A) Raster plots showing the post-stimulus timing of the spikes evoked by the six waveforms used in this study (insets). Dashed lines indicate stimuli transitions. (B–G) Post-stimulus histograms constructed out of the final 100 responses (gray bands and arrows indicate correspondence) to each stimulus waveform. (H,I) Mean latency (logarithmic scale) as a function of stimulus strength (rms value, logarithmic scale) for natural (H) and phase-transposed (I) stimuli. Note that there is the same difference in slope between responses to stimuli having θ_C (circles) and θ_R (squares) in the same plots (filled and open symbols correspond to H_R and H_C, respectively).

PM responses

All recorded PM afferents fired a single spike 1–2 ms after the stimulus without adaptation (Fig. 1A). The latency versus amplitude relationship was established based the response of different PMs to different stimulus amplitudes. Latency decreased with stimulus strength (Fig. 1H). Each receptor was only stimulated at a single amplitude but the obtained curve for each stimulus type shows a smooth hyperbolic course as expected if all receptors behave similarly.

For every receptor and stimulus strength, waveforms sharing the amplitude spectrum of the signal generated by capacitive objects [$H_C(\omega)$; Fig. 1H, open symbols] recruited spikes with shorter latency and smaller variability than those sharing the amplitude spectrum of the signal generated by resistive objects [$H_R(\omega)$; Fig. 1H, filled symbols]. Interestingly, latency and latency variability showed a strong correlation (Fig. 1I; Spearman correlation: ρ=0.9246).

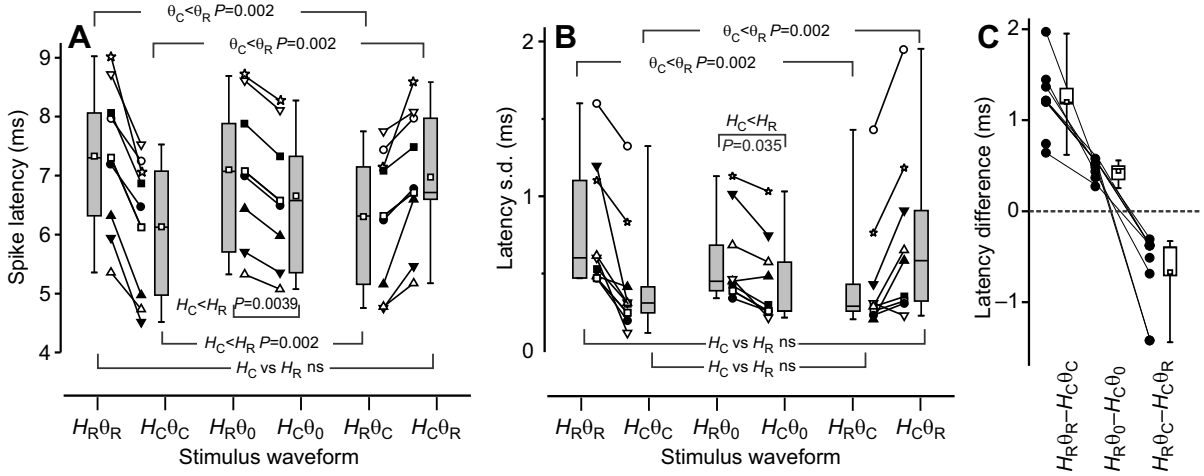

Fig. 4. BCs: first spike latency. (A) Mean latency of the earliest spike as a function of stimulus waveform (Friedman test: χ^2=38.27, d.f.=5, P=6.71×10^{-6}). Brackets indicate performed exact tests for the null hypotheses: 'responses to stimuli having $\theta_R(\omega)$ have equal or smaller latency than those having $\theta_C(\omega)$' (labeled $\theta_C<\theta_R$, P-values indicated in the figure, N=9, two tests, one-tail) and 'responses to stimuli having $H_R(\omega)$ have equal latency to those having $H_R(\omega)$' (significant differences at P_{HB}=0.05 were found for $H_R\theta_0$ versus $H_C\theta_0$ only, P=0.004, N=8, three tests). (B) Standard deviation of the latency of the earliest spike as a function of the stimulus waveforms (Friedman test: χ^2=27.5, d.f.=5, P=5.7×10^{-4}). Brackets indicate performed exact tests for testing the null hypotheses: 'responses to stimuli having $\theta_R(\omega)$ have equal or smaller latency variability than those having $\theta_C(\omega)$' (labeled $\theta_C<\theta_R$, P-values indicated in the figure, N=9, two tests) and 'responses to stimuli having $H_R(\omega)$ have equal latency variability to those having $H_R(\omega)$' (no significant differences at P_{HB}=0.05, N=8, three tests). (C) Difference between mean spike latencies evoked by stimuli having $H_R(\omega)$ and $H_C(\omega)$ (Friedman tests: χ^2=14, d.f.=2, P=9.1×10^{-4} ; *post-hoc* exact tests P=0.004, N=8, for each burst parameter as indicated by connecting lines in A, three tests). Symbols correspond to mean data for individually recorded units and the box and whisker plots are summaries. Numbers within the brackets in A and B are P-values before correction for multiple tests.

Journal of Experimental Biology (2019) 222, jeb191544. doi:10.1242/jeb.191544

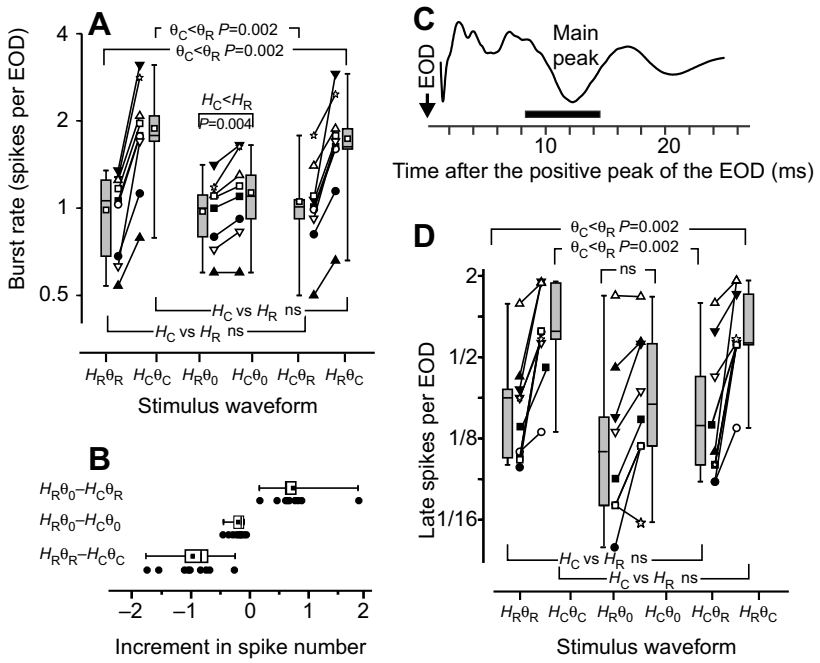

Fig. 5. BCs: spike number per electric organ discharge (EOD). (A) Total number of spikes in the burst per EOD (i.e. burst rate) as a function of stimulus waveform (Friedman test: χ^2=44.3, d.f.=5, P=4.9×10^{-7}). Brackets indicate performed exact tests for testing the null hypothesis 'stimuli having $\theta_R(\omega)$ have equal or larger burst rate than those having $\theta_C(\omega)$' (P=0.002, N=9, two tests, one-tail) and 'responses to stimuli having $H_R(\omega)$ have equal rate to those having $H_R(\omega)$' (significant differences at P_{HB}=0.05 were found for $H_R\theta_0$ versus $H_C\theta_0$ only; P=0.004, N=8, three tests). (B) Difference between mean number of spikes as a function of stimulus waveform (χ^2=18, d.f.=2, P=1×10^{-4}; P=0.004, N=8, three tests as indicated by connecting lines in A). (C) Field potentials recorded at the polymorphic cell layer of the centromedial map of the electrosensory lobe (data from Pereira et al., 2014). There are three main peaks at about 7, 12 and 23 ms after the EOD. (D) Spike number falling within the window 8–15 ms (marked with the black bar and potentially driving the 'center-on' pyramidal neurons, see Discussion) as a function of the stimulus waveforms (Friedman test: χ^2=38.9, d.f.=5, P=5.1×10^{-6}). Brackets indicate performed exact tests for testing the null hypotheses: 'responses to stimuli having $\theta_R(\omega)$ have an equal or larger number of spikes per EOD within the window than those having $\theta_C(\omega)$' (P=0.002, N=9) and 'responses to stimuli having $H_R(\omega)$ have an equal number of spikes per EOD to those having $H_R(\omega)$' (no significant differences at P_{HB}=0.05, N=8, three tests). Symbols correspond to mean data for individually recorded units and the box and whisker plots are summaries. Numbers within the brackets in A and D are P-values before correction for multiple tests.

There was a preferred order in the effectiveness of the tested waveforms (Fig. 2A; Friedman test, P=2.1×10^{-6}). *Post hoc* exact tests between responses to signals having either the same $H(\omega)$ or the same $\theta(\omega)$ indicate significant independent effects of phase (labeled as $\theta_C<\theta_R$) and amplitude spectra (labeled as $H_C<H_R$), respectively, on spike latency (P_{HB}<0.05). Differences between spike latencies were informative on the relative efficiency of $H(\omega)$ and $\theta(\omega)$. Latency differences between spikes evoked by stimuli reproducing natural fields ($H_C\theta_C$ and $H_R\theta_R$) were significantly larger than those evoked by stimuli having the same amplitude but zero-phase spectra ($H_C\theta_0$ and $H_R\theta_0$). These, in turn, were significantly larger than those evoked by stimuli having the same amplitude but phase-transposed spectra ($H_C\theta_R$ and $H_R\theta_C$; Fig. 2B). While the positive sign of these three differences (Fig. 2A; i.e. descending connecting lines, P_{HB}<0.05) indicates a predominant effect of amplitude spectra on the response of PMs, the decay of the differences in latency when phase spectra changed from natural to flat and then from flat to transposed (Fig. 2B; P_{HB}<0.05) indicates that they are also sensitive to the relative phase of the frequency components.

Consistently, ROC curves for stimuli having either the same amplitude or the same phase spectra showed that an external observer reading PM latency would discriminate amplitude spectra better than phase spectra. Fig. 2C,D shows example ROC curves obtained from the experiment in Fig. 1A. Areas under the ROC curves for discriminating between $H_R(\omega)$ and $H_C(\omega)$ (white bars in Fig. 2E) were significantly larger than those for discriminating between $\theta_R(\omega)$ and $\theta_C(\omega)$ (black and gray bars in Fig. 2E; P_{HB}<0.05).

BC responses

BC afferents fired a burst of spikes of high intrinsic frequency (up to 500 Hz) showing adaptation of the first spike latency and the total number of spikes per EOD (rate; Fig. 3A). Stimuli sharing $\theta_C(\omega)$ recruited BCs with earlier and stronger bursts than those sharing $\theta_R(\omega)$ or $\theta_0(\omega)$ (zero-phase spectrum) regardless of their amplitude spectra (post-stimulus histograms integrated the last 100 responses in the train to minimize the effect of adaptation in Fig. 3B–G). Mean latency systematically decreased with stimulus strength, following a hyperbolic course. Notably, latencies decreased faster in response to stimuli having θ_C (circles and dashed line, Fig. 3H,I) than to those having θ_R (squares and solid line, Fig. 3H,I), regardless of the $H(\omega)$ (encoded as filled and open symbols, Fig. 3H,I). As in the case of PMs, latency variability increased with latency when considering each receptor separately. However, the correlation between these two parameters was poor (Spearman correlation ρ=0.3727), suggesting receptor heterogeneity.

ANOVA followed by *post hoc* exact tests between responses having either the same $H(\omega)$ or the same $\theta(\omega)$ indicated significant effects of phase and amplitude spectra on the latency and latency variability of the first spike of the burst (Fig. 4A,B; P_{HB}<0.05). The differences between burst latency for stimuli having $H_C(\omega)$ and $H_R(\omega)$ were ordered identically depending on the phase spectrum for all recorded BCs (Fig. 4C). *Post hoc* exact tests showed that

Journal of Experimental Biology (2019) 222, jeb191544. doi:10.1242/jeb.191544

$H_C\theta_0$ evoked spikes significantly earlier than $H_R\theta_0$, indicating BC sensitivity to amplitude spectra (Fig. 4A,B, middle line series plots). Notably, the difference in mean latency was 1/3 of those observed for natural waveforms ($H_C\theta_C$ and $H_R\theta_R$; Fig. 4A,B, left line series plots), suggesting also a significant sensitivity to the phase spectrum. Confirming this hypothesis, stimulation with transposed phase spectra ($H_C\theta_R$ and $H_R\theta_C$; Fig. 4A,B, right line series plots) inverted the sign of the differences observed for natural stimuli (Fig. 4C; P_{HB}<0.05).

Similarly, ANOVA and *post hoc* tests showed that the number of spikes in the bursts evoked by signals with $\theta_C(\omega)$ were larger than those evoked by $\theta_R(\omega)$, indicating a predominant phase effect (P_{HB}<0.05). Differences between responses evoked by transposed stimuli having the same $\theta(\omega)$ were non-significant (i.e. P_{HB}>0.05) except in the case of $\theta_0(\omega)$. $H_C\theta_0$ evoked significantly stronger bursts than $H_R\theta_0$, indicating some BC sensitivity to amplitude spectra (Fig. 5A). However, the difference in spike number evoked by zero-phase stimuli was 1/5 of those observed for natural waveforms ($H_C\theta_C$ and $H_R\theta_R$, P_{HB}<0.05). Stimulation with transposed phase spectra ($H_C\theta_R$ and $H_R\theta_C$; Fig. 5B; P_{HB}<0.05) inverted the sign of the differences observed for natural stimuli.

Previous analyses led to the conclusion that stimuli having $\theta_C(\omega)$ evoked a burst starting about 1 ms earlier and firing about one spike more than those evoked by stimuli having $\theta_R(\omega)$. Responses to stimuli having θ_0 were intermediate.

Taking into account that the main peak of the field potentials and the peak of the post-stimulus histograms of center-on neurons (Krahe and Maler, 2014) evoked by the EOD in the electrosensory lobe falls beyond 9 ms after the EOD (Pereira et al., 2005, 2014; Fig. 5C) and that primary afferents converge on basilar dendrites of these neurons (Réthelyi and Szabó, 1973a; Maler, 1979, 2009a, b), we analyzed the responses of BC spikes that follow the first spike and fire within the window 8–15 ms. The responses evoked by stimuli having $\theta_C(\omega)$ showed a significantly larger number of spikes within the window than those having $\theta_R(\omega)$ for the same $H(\omega)$ (P_{HB}<0.05). Responses to stimuli having different $H(\omega)$ and the same $\theta(\omega)$ were not significantly different (P_{HB}=0.05).

Consistently with previous analysis, ROC curves for stimuli having either the same amplitude or the same phase spectrum indicated that an external observer reading either BC latency or BC rate would discriminate phase spectra better than amplitude spectra (Fig. 6). Areas under the ROC curves for discriminating between $H_R(\omega)$ and $H_C(\omega)$ (dark bars Fig. 6C,F) were significantly smaller than those for discriminating between $\theta_R(\omega)$ and $\theta_C(\omega)$ (white bars, Fig. 6C,F; P_{HB}<0.05).

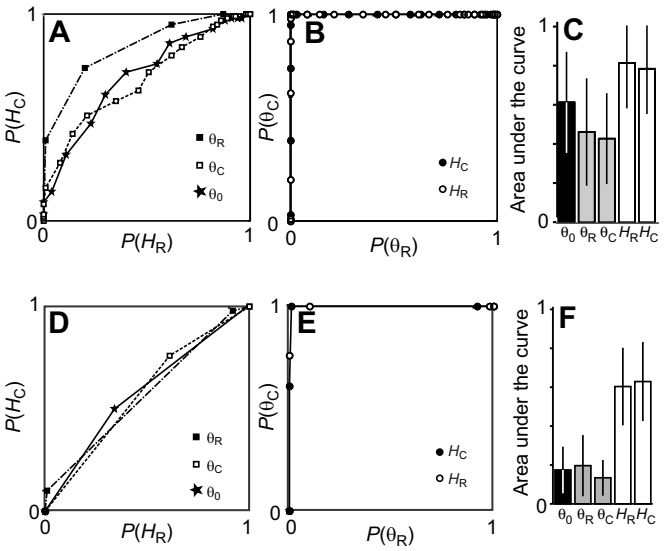

Fig. 6. ROC analysis for BCs. ROC curves in A, B, D and E correspond to the example shown in Fig. 3. A and D represent the probability that the amplitude spectrum of the stimulus is $H_C(\omega)$ {P[$H_R(\omega)$]} as a function of probability that it is $H_R(\omega)$ {P[$H_R(\omega)$]} when the burst has the same latency to the earliest spike (A) or rate (number of spikes in the burst; D) and the stimuli have either $\theta_C(\omega)$ (white squares), $\theta_R(\omega)$ (black squares) or $\theta_0(\omega)$ (stars) spectra. B and E represent the probability that the phase spectrum of the stimulus is $\theta_C(\omega)$ {P[$\theta_C(\omega)$]} as a function of probability that it is $\theta_R(\omega)$ {P[$\theta_C(\omega)$]} when the burst has the same latency (B) or rate (E) and the stimuli have either $H_C(\omega)$ (black circles) or $H_R(\omega)$ (white circles) spectra. (C,F) When considering all the studied population, areas under the ROC curves for phase discrimination (white bars) were significantly larger than those for amplitude discrimination (gray and black bars, Friedman tests χ^2=25.4, d.f.=4, P=4.2×10^{-5} and χ^2=27.3, d.f.=4, P=1.7×10^{-5} for latency and rate, respectively; the six possible *post hoc* exact tests were performed for each parameter, P=0.002, N=9). Lines correspond to s.d.

DISCUSSION

Here, we show that both types of tuberous primary afferents of the pulse-emitting fish *G. omarorum* respond to temporal cues embodied in the phase spectrum of electrosensory signals. While wave fish are mainly sensitive to the amplitude spectrum of the EOD (Hopkins, 1976), in *G. omarorum*, PMs and BCs are sensitive to both amplitude and phase spectra. Although the sensitivity spaces of both receptors are most likely overlapping, our experiments show that they are not identical. In fact, transposing spectra (i.e. combining H_R with θ_C and H_C with θ_R) causes qualitative differences between the responses of different afferent types. PMs are mainly driven by the amplitude spectrum and BCs by the phase spectrum of 'natural' stimuli generated by objects of different impedance.

For both receptor types, latency was a decreasing function of stimulus amplitude even though for each receptor we used a single amplitude. Latencies were much shorter for PMs than for BCs. This is probably associated to their difference in diameter and also with differences in the synaptic activation of the first Ranvier nodes of the afferents which are located differently, inside the receptor in PMs and outside in BCs (Echagüe and Trujillo-Cenóz, 1981; Caputi et al., 2002).

In PM afferents, the standard deviation and mean values of the latency of the single spike were strongly correlated, indicating a similar transmission delay, and suggesting a common encoding mechanism for the entire population. This was not the case for BCs, showing a poor correlation between the latency of the first spike and its variability. This is not surprising as, using other techniques, previous studies have sub-classified BCs into two or three types depending on the species and stimulus type used (Bastian, 1976; Watson and Bastian, 1979; Yager and Hopkins, 1993; McKibben et al., 1993). The sample size precludes us from advancing further in this aspect.

As in the auditory nerve of vertebrates (Heil, 2004) and sound detector afferents of insects (Pollack and Imaizumi, 1999), in PM and BC afferents, first spikes are precisely time locked to the stimulus and the variability of these responses to stimuli having the same energy content is sensitive to the stimulus quality. This is not the only similarity with the auditory system. As in audition (Heil, 2004; Hildebrandt, 2014; Pollack and Imaizumi, 1999), first spike latency and latency variability tend to be shortest at a specific frequency to which the afferent is most sensitive. In pulse Gymnotiformes, electroreceptor organs emit microphonic-like, so-called 'ringing' potentials, which consist of damped voltage oscillations between 800 and 900 Hz (Bennett, 1967; Castello

et al., 2000; Aguilera et al., 2001). These ringing potentials have been interpreted as originating in the pool of electrosensory cells inside the receptor capsule (Bennett, 1967; Cilleruelo and Caputi, 2012). They have a best frequency nearly duplicating the peak power frequency of the self-generated EOD in any natural condition (400–500 Hz). Signals evoked by capacitive objects shift up stimulus power density to frequencies closer to the ringing one and consequently the first spike latency and latency variability are reduced for stimuli of different quality and the same energy content. This may explain the sensitivity to the amplitude spectrum of both afferent types.

Transduction and encoding mechanisms in BCs appear to have additional components as they show a predominant responsiveness to the phase spectrum and also spike-time adaptation. In BCs, it appears that the entire phase spectrum affects the response of a single afferent, whereas amphibian auditory fibers show a single preferential stimulus phase for their best frequency (Hillery and Narins, 1987). Nonetheless, when the phase spectrum of a bullfrog's species-specific call was manipulated in an experiment similar to that described here, notable differences were found in primary afferent responses (Simmons et al., 1993). Although there are no physiological data at the cellular or subcellular level that can explain phase sensitivity at present, there are several well-documented anatomical differences in receptor organs including their size, fiber diameter (Szabó and Fessard, 1974) and branching patterns (Echagüe and Trujillo-Cenóz, 1981; Caputi et al., 2002) that should be taken into account to explain the different responses of BCs and PMs to the same stimulus.

Finally, intrinsic properties of BCs at the spike generator site (Benda et al., 2002) and synaptic dynamics appear to be the most probable mechanisms involved in bursting responses and in the power law spike rate adaptation shown by BCs. The latter is similar to that observed in wave fish (Benda et al., 2002; Clarke et al., 2013) and the auditory system (Benda and Hennig, 2008).

To understand how primary afferent signals are decoded in the next sensory processing stage, present knowledge on the electrosensory lobe of pulse Gymnotiformes should be taken into account. PMs and BCs give rise to separate electrosensory pathways converging at the mesencephalon (Carr et al., 1981; Szabó and Fessard, 1974; Carr and Maler, 1986). In turn, afferent fibers of both types trifurcate, generating three electrosensory maps (Heiligenberg and Dye, 1982; Shumway, 1989a, b; Maler, 2009a, b; Krahe and Maler, 2014). This implies that a single sensory physical image is transformed into six neural images, processed separately at the early sensory stages and combined downstream, probably at the torus semicircularis (Carr et al., 1981; Carr and Maler, 1986).

In the case of PM, latency and latency variability carry redundant information which may be integrated differently in three spherical neuron maps of the electrosensory lobe (Heiligenberg and Dye, 1982). PM branches project one-to-one onto the spherical neurons of the centromedial map, but converge on the same cell in the centrolateral and lateral maps (Castelló et al., 1998). Responsiveness of spherical neurons is dominated by a low-threshold slow-inactivating K^+ current and a mixed cation current, determining an onset phenotype (Nogueira et al., 2006; Nogueira and Caputi, 2014) similar to that observed in the auditory system of birds and mammals (Rathouz and Trussell, 1998; Bal and Oertel, 2001). Resonant currents reduce spherical cell input impedance and enhance the timing precision required for a latency code (Trussell, 1999; Nogueira and Caputi, 2011). In this readout context, one can postulate that centromedial spherical neurons represent the electric image of objects as a latency pattern, while at the lateral map, instead, spherical cells require synchronized input from multiple afferents from a larger region of the skin and may generate a reference signal that can be used downstream for latency decoding. In fact, all spherical neurons project to the magnocellularis nucleus where a Jeffress-like circuit has been described (pulse fish: Réthelyi and Szabó, 1973b; Sotelo et al., 1975; Matsushita et al., 2013; wave fish: Carr et al., 1981).

Regarding the readout circuit for BC afferents, it is known that they contact: (i) large multipolar and ovoid inhibitory neurons at the deep layer of the electrosensory lobe, (ii) granule cells and (iii) the basilar dendrites of center-on pyramidal cells (Réthelyi and Szabó, 1973a; Maler, 1979, 2009a, b). In addition, typical field potentials (Pereira et al., 2005, 2014) and post-EOD spike histograms of center-on units recorded in the electrosensory lobe of acute preparations and freely moving *G. omarorum* start firing at about 10 ms after the EOD, although some of them show a single occasional but phase-locked spikes between 5 and 7 ms (Pereira et al., 2014; Pereira Larronde, 2016; Rodríguez-Cattáneo, 2017). Moreover, almost complete silence in a sample of more than 200 neurons was recorded between 7 and 9 ms after the EOD (Pereira et al., 2014; Pereira Larronde, 2016; Rodríguez-Cattáneo, 2017). Taking this readout context into account, one must ask whether the role of all spikes in the burst is the same. In center-on pyramidal neurons, the excitatory post-synaptic potentials may evoke the early spike at 5–7 ms. However, synapses at the basilar dendrite are relatively far from the somata and basilar dendrites receive multiple inhibitory contacts from multipolar and ovoid neurons (Maler, 1979; Maler and Mugnaini, 1994; Berman and Maler, 1998a). Thus, cable properties of these dendrites, and consequently the amplitude and timing of the peaks of the afferent-evoked postsynaptic potentials at the spike generation site, are likely modulated by a feed-forward inhibition indirectly elicited by primary afferents via those deep inhibitory neurons. This indirect action of primary afferents may cause the strong silence observed in the field potentials and in most neurons of the electrosensory lobe between 7 and 9 ms after the EOD (Pereira et al., 2005, 2014). At the end of this inhibitory window, the remaining spikes in the BC burst are able to recruit pyramidal neurons generating the main peak of the field potentials at about 12–13 ms. BCs may also activate granular interneurons participating in inhibitory processes such as lateral inhibition and modulation of non-basilar pyramids in a way that is at present much less clear (Maler, 1979; Maler and Mugnaini, 1994; Berman and Maler, 1998b, 1999).

In consequence, while the effect of the first spike on center-on pyramidal neurons may be twofold, to gate the input at the basilar dendrites and also to generate lateral inhibition, the rest of the burst might drive center-on cells firing at about the main peak of the field potentials. In light of these hypotheses, the significant differences observed in the number of spikes in the window 8–15 ms after the EOD increases the evidence that the slow electrosensory path receives and processes information mainly encoded in the phase spectrum of the local EOD.

Conclusion

Active electroreception in pulse Gymnotiformes is a special case in which variations not only in the amplitude but also in the phase spectrum (e.g. in the whole waveform) of a self-generated stimulus are encoded by primary afferents. This form of encoding is qualitatively different from that observed in other senses in which receptor sensitivity either to the amplitude or to the phase spectrum is observed.

Visual color and sound timbre (in German, klangfarbe: sound color) are supported by receptor and primary afferent tuning to

frequency bands within the range of light (Wald, 1964) and sound (Hudspeth, 1989) spectra, respectively. Making an analogy, differential encoding in the fish may serve to encode the 'electric color' of the signals generated in the presence of complex impedance (Budelli and Caputi, 2000).

In pulse Mormyriformes, electroreceptors have a flat frequency sensitivity within a range of two orders of magnitude (Bell, 1990a, b). Thus, stimulus strength and phase spectrum may be considered the only two dimensions of a manifold where the 'electric color' of species, sex (Hopkins and Bass, 1981; Hopkins, 1986) and object impedance (von der Emde, 1990; von der Emde and Bleckmann, 1992; Gottwald et al., 2018) are represented. The present results show dual encoding of amplitude and phase spectral cues by each receptor type in *G. omarorum*. This may add a third dimension to the 'electric qualia' manifold used in object discrimination.

By the same token, and taking into account the differences in waveform of near electric fields generated by pulse Gymnotiformes (Aguilera et al., 2001; Rodríguez-Cattáneo et al., 2008, 2013; Castelló et al., 2009), the electroreceptor encoding of waveform described here could also be involved in the identification of species, sex, size and relative position of another weakly electric fish (Hopkins and Westby, 1986; McGregor and Westby, 1992).

Acknowledgements
Authors thank Dr Rafael Canetti for ongoing discussions and Ana Camargo for her technical assistance during the experiments.

Competing interests
The authors declare no competing or financial interests.

Author contributions
Conceptualization: A.A.C.; Methodology: A.A.C., P.A.A.; Software: A.A.C.; Validation: A.A.C., P.A.A.; Formal analysis: A.A.C., P.A.A.; Investigation: A.A.C., P.A.A.; Resources: A.A.C., P.A.A.; Data curation: A.A.C., P.A.A.; Writing - original draft: A.A.C., P.A.A.; Writing - review & editing: A.A.C., P.A.A.; Visualization: A.A.C., P.A.A.; Supervision: A.A.C.; Project administration: A.A.C.; Funding acquisition: A.A.C., P.A.A.

Funding
This work was partially funded by Programa de Desarrollo de las Ciencias Básicas (PEDECIBA) and Sistema Nacional de Investigadores, Uruguay (annual allowances to A.A.C. and P.A.A.).

Data availability
Stimulus waveforms, spike time stamps and processing codes are available on request from the authors (caputiangel@gmail.com or peaabar@gmail.com). Individual data points for response indicators are displayed on the figures.

References
Aguilera, P. A. and Caputi, A. A. (2003). Electroreception in *G. carapo*: detection of changes in waveform of the electrosensory signals. *J. Exp. Biol.* **206**, 989-998.
Aguilera, P. A., Castelló, M. E. and Caputi, A. A. (2001). Electroreception in *Gymnotus carapo*: differences between self-generated and conspecific-generated signal carriers. *J. Exp. Biol.* **204**, 185-198.
Assad, C., Rasnow, B. and Stoddard, P. K. (1999). Electric organ discharges and electric images during electrolocation. *J. Exp. Biol.* **202**, 1185-1193.
Bal, R. and Oertel, D. (2001). Potassium currents in octopus cells of the mammalian cochlear nucleus. *J. Neurophysiol.* **86**, 2299-2311.
Bastian, J. (1976). Frequency response characteristics of electroreceptors in weakly electric fish (Gymnotoidei) with a pulse discharge. *J. Comp. Physiol.* **112**, 165-180.
Bastian, J. (1977). Variations in the frequency response of electroreceptors dependent on receptor location in weakly electric fish (Gymnotoidei) with a pulse discharge. *J. Comp. Physiol.* **121**, 53-64.
Bell, C. C. (1990a). Mormyromast electroreceptor organs and their afferent fibers in mormyrid fish. II. Intra-axonal recordings show initial stages of central processing. *J. Neurophysiol.* **63**, 303-318.
Bell, C. C. (1990b). Mormyromast electroreceptor organs and their afferent fibers in mormyrid fish. III. Physiological differences between two morphological types of fibers. *J. Neurophysiol.* **63**, 319-332.
Bell, C. C. and Grant, K. (1989). Corollary discharge inhibition and preservation of temporal information in a sensory nucleus of mormyrid electric fish. *J. Neurosci.* **9**, 1029-1044.
Benda, J. and Hennig, R. M. (2008). Spike-frequency adaptation generates intensity invariance in a primary auditory interneuron. *J. Comp. Neurosci.* **24**, 113-136.
Benda, J., St-Hilaire, M. Herz, A. V. M. and Longtin, A. (2002). Effect of noise on the coding properties of two fundamental types of neurons. *Comp. Sci.* **2**, 1100-1105.
Bennett, M. V. L. (1967). Mechanisms of electroreception. In *Lateral Line Detectors* (ed. P. Cahn), pp. 313-393. Bloomington: Indiana University.
Bennett, M. V. L. and Grundfest, H., (1959). Electrophysiology of electric organ *in Gymnotus carapo*. *J. Gen. Physiol.* **42**, 1067-1104.
Berman, N. J. and Maler, L. (1998a). Distal versus proximal inhibitory shaping of feedback excitation in the electrosensory lateral line lobe: implications for sensory filtering.). *J. Neurophysiol.* **80**, 3214-3232.
Berman, N. J. and Maler, L. (1998b). Inhibition evoked from primary afferents in the electrosensory lateral line lobe of the weakly electric fish (Apteronotus leptorhynchus). *J. Neurophysiol.* **80**, 3173-3196.
Berman, N. J. and Maler, L. (1999). Neural architecture of the electrosensory lateral line lobe: adaptations for coincidence detection, a sensory searchlight and frequency-dependent adaptive filtering. *J. Exp. Biol.* 202, 1243-1253.
Budelli, R. and Caputi, A. A. (2000). The electric image in weakly electric fish: perception of objects of complex impedance. *J. Exp. Biol.* **203**, 481-492.
Caputi, A. A. (1999). The electric organ discharge of pulse gymnotiforms: the transformation of a simple impulse into a complex spatio-temporal electromotor pattern. *J. Exp. Biol.* **202**, 1229-1241.
Caputi, A., Macadar, O. and Trujillo-Cenóz, O. (1994). Waveform generation in *Rhamphichthys rostratus* (L.)(Teleostei, Gymnotiformes). *J. Comp. Physiol. A* **174**, 633-642.
Caputi, A. A., Silva, A. C. and Macadar, O. (1998). The electric organ discharge of *Brachyhypopomus pinnicaudatus*. *Brain. Behav. Evol.* **52**, 148-158.
Caputi, A. A., Castelló, M. E., Aguilera, P. and Trujillo-Cenóz, O. (2002). Electrolocation and electrocommunication in pulse gymnotids: signal carriers, pre-receptor mechanisms and the electrosensory mosaic. *J. Physiol.-Paris* **96**, 493-505.
Carr, C. and Maler, L. (1986). Electroreception in gymnotiform fish. Central anatomy and physiology. In: *Electroreception* (ed. T. H. Bullock and W. Heiligenberg), N.Y.: Willey and Sons.
Carr, C. E., Maler, L., Heiligenberg, W. and Sas, E. (1981). Laminar organization of the afferent and efferent systems of the torus semicircularis of gymnotiform fish: morphological substrates for parallel processing in the electrosensory system. *J. Comp. Neurol.* **203**, 649-670.
Castelló, M. E., Caputi, A. and Trujillo-Cenóz, O. (1998). Structural and functional aspects of the fast electrosensory pathway in the electrosensory lateral line lobe of the pulse fish *Gymnotus carapo*. *J. Comp. Neurol.* **401**, 549-563.
Castello, M. E., Aguilera, P. A., Trujillo-Cenoz, O. and Caputi, A. A. (2000). Electroreception in Gymnotus carapo: pre-receptor processing and the distribution of electroreceptor types. *J. Exp. Biol.* **203**, 3279-3287.
Castelló, M. E., Rodríguez-Cattáneo, A., Aguilera, P. A., Iribarne, L., Pereira, A. C. and Caputi, Á. A. (2009). Waveform generation in the weakly electric fish *Gymnotus coropinae* (Hoedeman): the electric organ and the electric organ discharge. *J. Exp. Biol.* **212**, 1351-1364.
Cilleruelo, E. R. and Caputi, Á. A. (2012). Encoding electric signals by *Gymnotus omarorum*: heuristic modeling of tuberous electroreceptor organs. *Brain Res.* **1434**, 102-114.
Clarke, S. E., Naud, R., Longtin, A. and Maler, L. (2013). Speed-invariant encoding of looming object distance requires power law spike rate adaptation. *PNAS* **110**, 13624-13629.
Eastman, G., Valiño, G., Radío, S., Quintana, L., Young, R. L., Zakon, H. H., Hofmann, H. A., Sotelo-Silveira, J. and Silva, A. (2018). Sociogenomics of the dominant subordinate status in the weakly electric fish, *Gymnotus omarorum*. International Congress of Neuroethology 2018, 9th Electric Fish Meeting.
Echagüe, A. and Trujillo-Cenóz, O. (1981). Innervation patterns in the tuberous organs of *Gymnotus carapo*. In *Sensory Physiology of Aquatic Lower Vertebrates* (ed. T. Szabó and G. Czéh), pp. 29-40. Elsevier.
Gottwald, M., Singh, N., Haubrich, A. N., Regett, S. and von der Emde, G. (2018). Electric-color sensing in weakly electric fish suggests color perception as a sensory concept beyond vision. *Curr. Biol.* **28**, 3648-3653.e2.
Heil, P. (2004). First-spike latency of auditory neurons revisited. *Curr. Op. Neurobiol.* **14**, 461-467.
Heiligenberg, W. and Altes, R. A. (1978). Phase sensitivity in electroreception. *Science* **199**, 1001-1004.
Heiligenberg, W. and Dye, J. (1982). Labelling of electroreceptive afferents in a gymnotoid fish by intracellular injection of HRP: the mystery of multiple maps. *J. Comp. Physiol.* **148**, 287-296.
Hildebrandt, K. J. (2014). Neural maps in insect versus vertebrate auditory systems. *Curr. Op. Neurobiol* **24**, 82-87.

Hillery, C. M. and Narins, P. M. (1987). Frequency and time domain comparison of low-frequency auditory fiber responses in two anuran amphibians. *Hearing Res.* **25**, 233-248.
Hopkins, C. D. (1976). Stimulus filtering and electroreception: tuberous electroreceptors in three species of gymnotoid fish. *J. Comp. Physiol.* **111**, 171-207.
Hopkins, C. D. (1986). Temporal structure of non-propagated electric communication signals. *Brain. Behav. Evol.* **28**, 43-59.
Hopkins, C. D. and Bass, A. H. (1981). Temporal coding of species recognition signals in an electric fish. *Science* **212**, 85-87.
Hopkins, C. D. and Westby, G. W. M. (1986). Time domain processing of electric organ discharge waveforms by pulse-type electric fish. *Brain Behav. Evol.* **29**, 77-104.
Hudspeth, A. J. (1989). How the ear's works work. *Nature* **341**, 397.
Kawasaki, M. (2005). Physiology of Tuberous Electrosensory Systems. In *Electroreception. Springer Handbook of Auditory Research*, vol. 21 (ed. T.H. Bullock, C.D. Hopkins, A.N. Popper, R.R. Fay), pp. 154-194. New York, NY: Springer.
Krahe, R. and Maler, L. (2014). Neural maps in the electrosensory system of weakly electric fish. *Curr. Op. Neurobiol.* **24**, 13-21.
Maler, L. (1979). The posterior lateral line lobe of certain gymnotoid fish: quantitative light microscopy. *J. Comp. Neurol.* **183**, 323-363.
Maler, L. (2009a). Receptive field organization across multiple electrosensory maps. I. Columnar organization and estimation of receptive field size. *J. Comp. Neurol.* **516**, 376-393.
Maler, L. (2009b). Receptive field organization across multiple electrosensory maps. II. Computational analysis of the effects of receptive field size on prey localization. *J. Comp. Neurol.* **516**, 394-422.
Maler, L. and Mugnaini, E. (1994). Correlating gamma-aminobutyric acidergic circuits and sensory function in the electrosensory lateral line lobe of a gymnotiform fish. *J. Comp. Neurol.* **3452**, 224-252.
Matsushita, A., Pyon, G. and Kawasaki, M. (2013). Time disparity sensitive behavior and its neural substrates of a pulse-type gymnotiform electric fish, *Brachyhypopomus gauderio*. *J. Comp. Physiol. A* **199**, 583-599.
McGregor, P. K. and Max Westby, G. W. (1992). Discrimination of individually characteristic electric organ discharges by a weakly electric fish. *Animal Behav.* **43**, 977-986.
McKibben, J. R., Hopkins, C. D. and Yager, D. D. (1993). Directional sensitivity of tuberous electroreceptors: polarity preferences and frequency tuning. *J. Comp. Physiol.* **173**, 415-424.
Müller, J. (1837). *Handbuch der Physiologie des Menschen für Vorlesungen*, Vol. 1, 3rd edn. Koblenz, Verlag von J. Hölscher.
Nogueira, J. and Caputi, Á. A. (2011). Timing actions to avoid refractoriness: a simple solution for streaming sensory signals. *PLoS One* **6**, e22159.
Nogueira, J. and Caputi, A. A. (2014). Pharmacological study of the one spike spherical neuron phenotype in *Gymnotus omarorum*. *Neuroscience* **258**, 347-354.
Nogueira, J., Castelló, M. E. and Caputi, A. A. (2006). The role of single spiking spherical neurons in a fast sensory pathway. *J. Exp. Biol.* **.209**, 1122-1134.
Palmer, S. E. (1999). *Vision science: Photons to phenomenology*. MIT Press.
Pereira Larronde, A. C. (2016). Evidencias de la naturaleza háptica del sentido eléctrico activo en peces. *PhD Thesis*, PEDECIBA, Montevideo, Uruguay.
Pereira, A. C. and Caputi, A. A. (2010). Imaging in electrosensory systems. *Interdis. Sci.: Comp. Life Sci.* **2**, 291-307.
Pereira, A. C., Centurion, V. and Caputi, A. A. (2005). Contextual effects of small environments on the electric images of objects and their brain evoked responses in weakly electric fish. *J. Exp. Biol.* **208**, 961-972.
Pereira, A. C., Rodríguez-Cattáneo, A. and Caputi, A. A. (2014). The slow pathway in the electrosensory lobe of Gymnotus omarorum: Field potentials and unitary activity. *J. Physiol.-Paris* **108**, 71-83.
Pollack, G. S. and Imaizumi, K. (1999). Neural analysis of sound frequency in insects. *BioEssays* **21**, 295-303.
Rathouz, M. and Trussell, L. (1998). Characterization of outward currents in neurons of the avian nucleus magnocellularis. *J. Neurophysiol.* **80**, 2824-2835.
Réthelyi, M. and Szabó, T. (1973a). Neurohistological analysis of the lateral lobe in a weakly electric fish, *Gymnotus carapo* (Gymnotidae, Pisces). *Exp. Brain Res.* **18**, 323-339.
Réthelyi, M. and Szabó, T. (1973b). A particular nucleus in the mesencephalon of a weakly electric fish, gymnotus carapo, gymnotidae. *Exp. Brain Res* **17**, 229-241.
Richer-de-Forges, M. M., Crampton, W. G. R. and Albert, J. S. (2009). A new species of Gymnotus (Gymnotiformes, Gymnotidae) from Uruguay: description of a model species in neurophysiological research. *Copeia* **3**, 538-544.
Rodríguez-Cattáneo, A. (2017). Codificación electrosensorial temprana en peces eléctricos de pulso. *PhD thesis*, PEDECIBA, Montevideo, Uruguay.
Rodríguez-Cattáneo, A., Pereira, A. C., Aguilera, P. A., Crampton, W. G. R. and Caputi, A. A. (2008). Species-specific diversity of a fixed motor pattern: the electric organ discharge of Gymnotus. *PLoS One* **3**, e2038.
Rodríguez-Cattáneo, A., Aguilera, P., Cilleruelo, E., Crampton, W. G. and Caputi, A. A. (2013). Electric organ discharge diversity in the genus Gymnotus: anatomo-functional groups and electrogenic mechanisms. *J. Exp. Biol.* **216**, 1501-1515.
Rodríguez-Cattáneo, A., Aguilera, P. A. and Caputi, A. A. (2017). Waveform sensitivity of electroreceptors in the pulse weakly electric fish Gymnotus omarorum. *J. Exp. Biol.* **220**, 1663-1673.
Scheich, H., Bullock, T. H. and Hamstra, R. H., Jr (1973). Coding properties of two classes of afferent nerve fibers: high-frequency electroreceptors in the electric fish, Eigenmannia. *J. Neurophysiol.* **36**, 39-60.
Shumway, C. A. (1989a). Multiple electrosensory maps in the medulla of weakly electric gymnotiform fish. I. Physiological differences. *J. Neurosci.* **9**, 4388-4399.
Shumway, C. A. (1989b). Multiple electrosensory maps in the medulla of weakly electric gymnotiform fish. II. Anatomical differences. *J. Neurosci.* **9**, 4400-4415.
Simmons, A. M., Reese, G. and Ferragamo, M. (1993). Periodicity extraction in the anuran auditory nerve. II: Phase and temporal fine structure. *J. Acoust. Soc. Am.* **93**, 3374-3389.
Sotelo, C., Réthelyi, M. and Szabó, T. (1975). Morphological correlates of electrotonic coupling in the magnocellular mesencephalic nucleus of the weakly electric fish *Gymnotus carapo*. *J. Neurocytol.* **4**, 587-607.
Stoddard, P. K., Rasnow, B. and Assad, C. (1999). Electric organ discharges of the gymnotiform fishes: III. Brachyhypopomus. *J. Comp. Physiol. A* **184**, 609-630.
Szabo, T. and Fessard, A. (1974). Physiology of electroreceptors. In *Electroreceptors and Other Specialized Receptors in Lower Vertebrates* (ed. A. Fessard), pp. 60-124. Springer.
Trussell, L. O. (1999). Synaptic mechanisms for coding timing in auditory neurons. *Ann. Rev. Physiol.* **61**, 477-496.
Viancour, T. A. (1979). Electroreceptors of a weakly electric fish. *J. Comp. Physiol.* **133**, 327-338.
von der Emde, G. (1990). Discrimination of objects through electrolocation in the weakly electric fish, Gnathonemus petersii. *J. Comp. Physiol. A.* **167**, 413-421.
von der Emde, G. and Bleckmann, H. (1992). Differential responses of two types of electroreceptive afferents to signal distortions may permit capacitance measurement in a weakly electric fish, Gnathonemus petersii. *J. Comp. Physiol. A.* **171**, 683-694.
Von der Emde, G. and Ronacher, B. (1994). Perception of electric properties of objects in electrolocating weakly electric fish: two-dimensional similarity scaling reveals a City-Block metric. *J. Comp. Physiol. A* **175**, 801-812.
Waddell, J. C., Rodríguez-Cattáneo, A., Caputi, A. A. and Crampton, W. G. R., (2016). Electric organ discharges and near-field spatiotemporal patterns of the electromotive force in a sympatric assemblage of Neotropical electric knifefish. *J. Physiol.-Paris* **110**, 164-181.
Wald, G. (1964). The receptors of human color vision. *Science* **145**, 1007-1016.
Watson, D. and Bastian, J. (1979). Frequency response characteristics of electroreceptors in the weakly electric fish, *Gymnotus carapo*. *J. Comp. Physiol.* **134**, 191-202.
Yager, D. D. and Hopkins, C. D. (1993). Directional characteristics of tuberous electroreceptors in the weakly electric fish, Hypopomus (Gymnotiformes). *J. Comp. Physiol.* **173**, 401-414.
Zakon, H. H. (1986). The electroreceptive periphery. In *Electroreception* (ed. T. H. Bullock and W. Heiligenberg), pp. 103-156. New York: John Willey & Sons.